Earth and Planetary Physics
地球与行星物理
ISSN 2096-3955
CN 10-1502/P

Large-scale episodic enhancements of relativistic electron intensities in Jupiter's radiation belt

ChongJing Yuan , YiQiao Zuo , Elias Roussos , Yong Wei , YiXin Hao , YiXin Sun , and Norbert Krupp

Citation: (2021). Large-scale episodic enhancements of relativistic electron intensities in Jupiter's radiation belt. *Earth Planet. Phys.*, *5*(4), 1−13. https://doi.org/10.26464/epp2021037

RESEARCH ARTICLE
PLANETARY SCIENCES

Earth and Planetary Physics
5: 314–326, 2021
doi: 10.26464/epp2021037

Large-scale episodic enhancements of relativistic electron intensities in Jupiter's radiation belt

ChongJing Yuan[1,2,3], YiQiao Zuo[1,2,3], Elias Roussos[4*], Yong Wei[1,2,3], YiXin Hao[5], YiXin Sun[5], and Norbert Krupp[4]

[1]Key Laboratory of Earth and Planetary Physics, Institute of Geology and Geophysics, Chinese Academy of Sciences, Beijing 100029, China;

[2]Innovation Academy for Earth Science, Chinese Academy of Sciences, Beijing 100029, China;

[3]University of Chinese Academy of Sciences, Beijing 100049, China;

[4]Max Planck Institute for Solar System Research, Justus-von-Liebig-Weg 3, Göttingen, 37077, Germany;

[5]Institute of Space Physics and Applied Technology, Peking University, Beijing 100871, China

Key Points:

- Seven transient enhancement events of relativistic electrons are identified from Galileo's observations, and an average recurrence time scale of a few days is resolved.
- Transient events mainly occur at 20 ± 5R_J with a remarkable feature of dawn-dusk asymmetry.
- Transient events may result from a synergy between the convective transport due to a dawn-dusk electric field and injections in the middle magnetosphere.

Citation: Yuan, C. J., Zuo, Y. Q., Roussos, E., Wei, Y., Hao, Y. X., Sun, Y. X. and Krupp, N. (2021). Large-scale episodic enhancements of relativistic electron intensities in Jupiter's radiation belt. *Earth Planet. Phys.*, *5*(4), 314–326. http://doi.org/10.26464/epp2021037

Abstract: Previous studies indicate that, in the Jovian magnetosphere, the long-term trend of the radial profile of relativistic electron intensities is primarily shaped by slow radial diffusion. However, measurements by the Galileo spacecraft reveal the existence of transient increases in MeV electron intensities well above the ambient distribution. It is unclear how common such transient enhancements are, and to which dynamic processes in Jupiter's magnetosphere their occurrence is linked. We investigate the radial distributions of >11 MeV and >1 MeV electron intensities from 9R_J to 40R_J (R_J = 71492 km denotes the Jovian radius), measured by the Galileo spacecraft from 1996 to 2002. We find transient enhancements of MeV electrons during seven Galileo crossings, mostly occurring around ~20R_J. An apparent dawn-dusk asymmetry of their occurrence is resolved, with a majority of events discovered at dawn. This dawn-dusk asymmetry, as well as the average recurrence time scale of a few days, implies a potential relationship between the MeV electron transients and the storm-like dynamics in the middle and outer magnetosphere detected using a variety of Galileo, Juno and remote sensing aurora observations. We suggest that the observations of some of these transients in the inner magnetosphere may result from a synergy between the convective transport by a large-scale dawn-dusk electric field and the sources provided by injections in the middle magnetosphere.

Keywords: radiation belt; Jupiter; relativistic electrons; magnetosphere

1. Introduction

The inner radiation belt of relativistic electrons trapped at < 5R_J (R_J = 71492 km denotes the Jovian radius) in Jovian magnetosphere was discovered through the remote sensing of synchrotron emissions in the decimetric wavelength band (Drake & Hvatum, 1959; Bolton et al., 2002). In-situ measurements during the flybys by the Pioneer spacecraft revealed that strong relativistic electron intensities extend to the middle magnetosphere (Simpson et al., 1974; Fillius & McIlwain, 1974). Then came the era of Galileo mission, in which the orbiter facilitated the first investigation of the evolution and dynamics of the radiation environment of subrelativistic to ultrarelativistic electrons around the magnetic equatorial plane.

Sorensen et al. (2005) and Jun et al. (2005) investigated long-term trends in the radial distributions of multi-MeV electrons in the Jovian magnetosphere observed by Galileo. The long-term median of the radial profiles of >1 MeV and >11 MeV electron intensities at 9–40R_J displayed a decreasing monotonic trend with increasing radial distance, with a change in the decreasing slope to be less steep beyond ~20R_J (Sorensen et al., 2005). Kollmann et al. (2018) analyzed variations in the key parameters of electron spectra with L (L denotes L-shell, which is defined as the radial distance of the equatorial crossing of magnetic field lines in units of R_J). The authors determined that the evolution of mission-averaged spectra parameters from the outer Jovian magnetosphere down to at least L = 20 matches the prediction of adiabatic heating theory. Garrett and Jun (2021) calculated the phase space densities (PSD) of multi-MeV electrons. Through the radial profiles

Correspondence to: E. Roussos, roussos@mps.mpg.de
Received 19 MAR 2021; Accepted 02 JUN 2021.
Accepted article online 18 JUN 2021.

of PSD at L = 8–25, the authors demonstrated that radial diffusion acts as the major process shaping the equilibrium structure of relativistic electron radiation.

However, inspection of individual Galileo orbits reveals that the MeV electron radial profiles are highly variable (Sorensen et al., 2005). Of particular interest is the enhancement of extended (> 1R_J) relativistic electron intensities standing out from the ambient radiation belt distribution. Roussos et al. (2018) discussed one such typical enhancement case of >11 MeV electron intensities during orbit C22, previously reported by several studies (Russell et al., 2001; Sorensen et al., 2005). The C22 event is morphologically similar to the enhancement of MeV electrons, i.e., transient extensions, frequently observed in the Kronian electron radiation belt (Roussos et al., 2018; Yuan et al., 2020). Roussos et al. (2018), Hao et al. (2020), Sun et al. (2019) and Yuan et al. (2020) proposed that a potential mechanism for the transient extensions is an energy dependent adiabatic acceleration associated with convective transport, due to large-scale noon-midnight electric fields in Saturn's magnetosphere (Paranicas et al., 2010; Thomsen et al., 2012; Andriopoulou et al., 2012, 2014). The existence of a similar large-scale electric field in Jupiter's magnetosphere, albeit in the dawn-dusk direction, has been inferred from the local time (LT) asymmetry of extreme ultraviolet (EUV) emissions of the Io plasma torus (IPT) (Barbosa & Kivelson, 1983; Ip & Goertz, 1983; Murakami et al., 2016). Hao et al. (2020) reconstructed several key characteristics of the C22 event in the Jovian radiation belt based on the scenario of convective transport due to a variable dawn-dusk electric field (Murakami et al., 2016).

Considering the findings in Saturn's radiation belts and those for Jupiter by Hao et al. (2020), it seems peculiar that only one event like C22 was captured by Galileo. For this reason, we perform a fresh survey of Galileo's seven years of observations to explore the dynamic processes that may generate the Jovian counterparts of transient extensions. In Section 2, we introduce the instrument and dataset employed in this study. Then we present case studies of transient extension events, as well as statistical analyses in Section 3. Extended discussion and conclusions are given in Sections 4 and 5, respectively.

2. Instruments and Dataset

The Galileo spacecraft orbited Jupiter at low-inclination trajectories for approximately seven years from 1995–2002. The orbiter carried an Energetic Particle Detector (EPD) which consisted of two double-headed detectors: the Low Energy Magnetospheric Measurement System (LEMMS) and the Composition Measurement System (CMS). The EPD measured the intensity of energetic charged particles from tens of keV to several MeV, as well as determining particle species. A detailed description of the instrument can be found in Williams et al. (1992), and a more up-to-date User Manual is provided by Kollmann et al. (2020). Due to the failed deployment of Galileo's high-gain antenna, most data could only be obtained in the real-time mode with low time resolution (minutes for MeV electrons), except during close moon flybys and other periods when EPD operated in record mode with high time resolution (seconds).

We mainly utilized LEMMS measurements of the intensities of energetic and relativistic electrons. For energies ranging higher than 1 MeV, LEMMS was not able to directly infer differential intensities, only measuring integral count-rates. We use the omnidirectional integral count-rates from two integral channels, DC3 (>11 MeV) and DC2 (>1 MeV), of LEMMS's High Energy Telescope (HET). We note that differential flux intensities of MeV electrons may be obtained, but it requires assumptions on electron energy spectra and further processing through simulations. Thus we choose to keep the raw count-rates for the analyses of MeV electrons, so that our conclusions are less dependent on the spectral shape assumptions (Kollmann et al., 2020).

For electrons with energies less than 1 MeV, the LEMMS's Low Energy Telescope (LET) provides measurements of differential intensities. The differential channels investigated in this study are F0, F1, F2, and F3, of which the energy passbands are 93–188, 174–304, 304–527, and 527–884 keV, respectively. These F channels are subject to contamination by penetrating MeV electrons, but the differential fluxes provided in the dataset have been cleaned, calibrated, and adjusted for other effects such as dead time (Kollmann et al., 2020). Thus, we base our analysis on the differential fluxes of the F channels (instead of the raw count-rates) since their estimation is less ambiguous.

3. Observations

We systematically investigated the distributions of >11 and >1 MeV electron count-rates between the radial distances of 9R_J to 40R_J. We consider here the Jovicentric radial distance rather than L-shell, as precise magnetic mapping offers no advantage for the present study. On the one hand, the magnetic field lines become increasingly stretched outward of ~20R_J; consequently, the L-shell derived from a magnetic field model becomes less accurate, even at magnetic latitudes with only a small offset from the magnetic equator. On the other hand, the distance range of transient extensions eventually revealed by measurements is inward of ~25R_J, where the magnetic equatorial crossings of Galileo are approximately indicative of the L-shell range involved.

Figure 1 presents the typical case of >11 MeV transient extension during orbit C22. A strong increase in the >11 MeV count-rates can be found outward of ~13R_J during the inbound crossing (red profile), constituting the C22 event mentioned in the introductory section. The black profile shows the long-term averaged count-rate at each radial distance, representing the average environment along Jupiter's equatorial plane, or the quiet-time state. The relativistic electron count-rates monotonically decrease with increasing radial distance. The monotonic outbound profile during orbit C22 (blue line) is more typical of the average radial distribution (Kollmann et al., 2018), with the superimposed sinusoidal variations from the few-degree excursions of Galileo above and below the magnetic equator due to the rotational wobbling of Jupiter's magnetic field.

3.1 Event Definition and Identification

We survey each Galileo orbit separately to obtain an average profile, which is constructed by combining the inbound and outbound segments of the current orbit. For a case to be considered

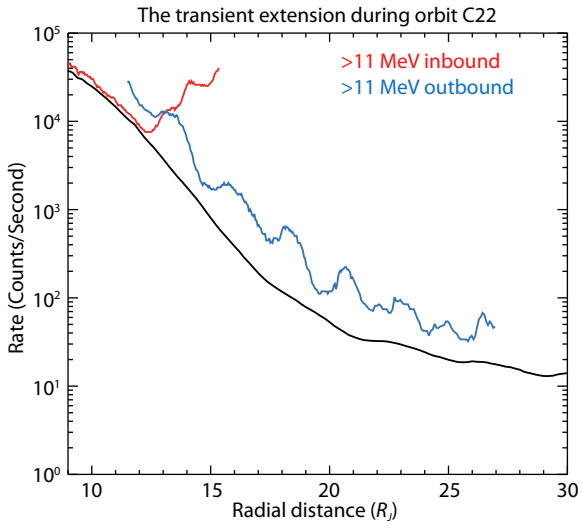

Figure 1. The radial distributions of >11 MeV electron count-rates during the inbound and outbound crossings of orbit C22, represented by the red and blue profiles, respectively. The black profile shows the long-term averaged count-rate at each radial distance, representing the average environment along Jupiter's equatorial plane.

a transient extension event, the peak enhancement in its radial profile should be ≳ 1 order of magnitude greater than the average profile, and the full width at 10% maximum should span > 1R_J in the radial distance. 10% maximum is used so as to capture the full breadth of the transient. Below 10%, the boundaries between the transient and the quiet magnetosphere are less precisely defined.

Table 1 shows all seven Galileo crossings during which we found transient extension events. Note that when we identify a transient event, we consider not only the Galileo crossing during which the event occurred, but also the electron energy channel involved. Thus, if during a single crossing, both the >1 MeV and >11 MeV channels fulfill our event definition, we consider that there are two transient events. For each crossing, we have listed the details about the location and intensity of the transient, together with the energy channel dominating the event. The latter is decided by a parameter γ shown in the last column of Table 1, which is the ratio of DC3 to DC2 rates at the radial distance of peak count-rate for the transient event, normalized by the long-term average ratio at the same radial distance. The normalization is applied because we want to remove the trend resulting from spatial variation, in order to show only the temporal changes. γ much larger (smaller) than 1 indicates that the transient event is dominated by >11 MeV (>1 MeV) electrons, whereas γ close to 1 indicates that the contributions from >11 MeV and from >1 MeV electrons are the same.

As shown in Table 1, γ is 17.6 and 15.0 for the transients during the outbound crossing of orbit E6 and inbound crossing of orbit C22, respectively, indicating that these two events are dominated by >11 MeV electrons. For the transient events during the inbound crossings of orbits E4 and E6 and for the outbound crossing of orbit I24, γ is 0.4, 0.2 and 0.3, respectively. Thus, these transients are dominated by >1 MeV electrons. For the inbound crossings of orbits C9 and E17, γ is 0.9 and 1.7, respectively, which means that for these two events, >11 MeV and >1 MeV electrons are about equally important.

3.2 Case Studies

3.2.1 Orbit E6: from inbound crossing with enhancement at >1 MeV to outbound crossing with enhancement at >11 MeV

Figure 2a shows the transient extension at >1 MeV during the inbound crossing of orbit E6 at the dawn sector with LT ~7 h from 4:21 to 9:33 in day 50 of 1997. The peak enhancement of >1 MeV rates occurs at ~22R_J, spanning about 2R_J in radial distance (bounded by the two vertical dashed lines marked with L2 and L3). The peak count-rate of this event is about 34 times above the average rate at the same radial distance. The parameter γ is about

Table 1. The transient extensions: Galileo orbit, time, energy, location and count-rate intensity.

Orbit	Time[1]	Energy	L_{Cmax}[2]	Full Width 10%Maximum[3]	LT_{Cmax}[4]	Cmax[5]	$\frac{Cmax}{Cavg}$[6]	γ[7]
E4 inbound	1996-352 08:24-12:23	>1 MeV	23.47	1.57	7.96	32942.42	12.60	0.4
E6 inbound	1997-050 04:21-09:33	>1 MeV	22.33	2.00	7.30	107007.30	33.66	0.2
E6 outbound	1997-053 00:56-11:57	>11 MeV	18.95	4.51	21.05	4363.99	50.82	17.6
C9 inbound	1997-176 09:38 to 1997-177 03:14	>11 MeV	27.02	7.00	5.43	971.15	44.87	0.9
	1997-176 09:38 to 1997-177 03:14	>1 MeV	22.95	7.00	6.02	120651.10	37.15	0.9
E17 inbound	1998-268 05:04-07:33	>11 MeV	18.01	1.11	5.34	4375.73	43.40	1.7
	1998-268 05:20-08:11	>1 MeV	18.21	1.28	5.29	352651.90	24.16	1.7
C22 inbound	1999-223 14:05-19:52	>11 MeV	15.34	3.18	3.29	40370.54	74.84	15.0
I24 outbound	1999-285 01:44-05:50	>1 MeV	18.47	2.10	16.81	110605.90	7.88	0.3

[1] Time: The UT time of the detection of the transient event, decided according to the transient's peak count-rate location and its width (refer to Full Width 10%Maximum in this table) in radial distance. The time format is yyyy-doy hh:mm. [2] L_{Cmax} (R_J): the location of transient's peak count-rate in the radial distance. [3] Full Width 10%Maximum (R_J): Full width of 10% peak count-rate in radial distance. [4] LT_{Cmax} (Hour): the location of transient's peak count-rate in local time. [5] Cmax (s^{-1}): the peak count-rate of transient extension. [6] $\frac{Cmax}{Cavg}$: Cmax normalized by the long-term average rate at L_{Cmax}. [7] γ: the ratio of >11 MeV to >1 MeV count-rates at L_{Cmax} normalized by the long-term average ratio at L_{Cmax}.

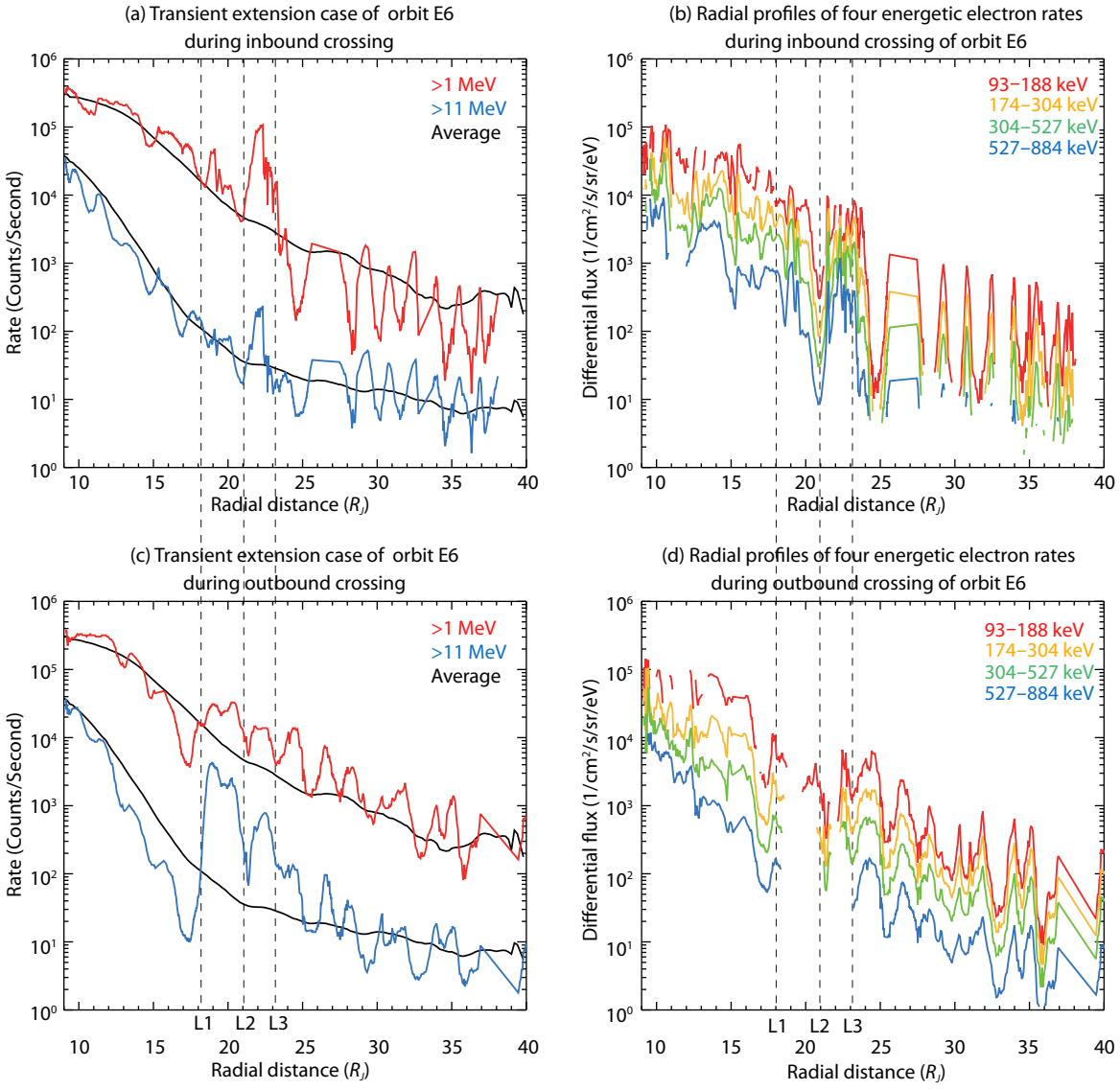

Figure 2. The transient extensions during orbit E6. (a) and (b): The radial distribution of the electron intensities from day 48 to 51 in 1997 during the inbound crossing. (c) and (d): The radial distribution of electron intensities from day 51 to 55 in 1997 during the outbound crossing. For panels (a) and (c), the red profiles indicate count-rates from channel DC2 (>1 MeV), while the blue ones are count-rates from channel DC3 (>11 MeV). The upper and lower black profiles in each panel indicate the long-term average rates of channels DC2 and DC3, respectively. For panels (b) and (d): The red, orange, green, and blue lines depict the differential flux intensities of channels F0, F1, F2, and F3 (93–188, 174–304, 304–527, and 527–884 keV), respectively. The three vertical dashed lines marked L1, L2, and L3 denote the radial distance of transient extensions.

0.2, which means this event is dominated by >1 MeV electrons. Meanwhile, a much reduced increase of >11 MeV electrons appears at the same radial distance, indicating that the enhancement is not narrowly confined in energy. Beyond ~25R_J, the relativistic and energetic electron intensities present periodic oscillations, with a period of approximately 10 hours. The oscillation in rates results from the few degree excursions of Galileo above and below the magnetic equator due to the rotational wobbling of Jupiter's magnetic field (Northrop et al., 1974; Khurana, 1992), and do not correspond to transients. The oscillations reflect the latitudinal distribution of relativistic elections, not the result of perturbations due to dynamic processes. We find that the envelope of the peaks still presents the trend of monotonic decrease, consistent with the quiet-time state indicated by the long-term average profile (solid black lines).

Figure 2b shows the corresponding radial profiles of energetic electron differential fluxes from channels F0, F1, F2, and F3 (93–188, 174–304, 304–527 and 527–884 keV), as indicated by the red, orange, green, and blue colors, respectively. We present the measurements of sub-MeV electrons in order to explore the possible sources of the transient events. As demonstrated in Kollmann et al. (2018), the sub-MeV electrons in the middle magnetosphere are dominated by adiabatic acceleration coupled with injections associated with reconnection and interchange processes, or radial diffusion. These sub-MeV electrons may be further accelerated to MeV energies and serve as the seed population of the transients. Figure 2b shows that at ~22R_J where the >1 MeV transi-

ent exists, there are simultaneous enhancements in these four energetic electron channels.

Figure 2c shows the transient event of >11 MeV electrons during the outbound crossing of the same orbit. After ~2.6 days from the detection of the transient extension at >1 MeV, when Galileo returns to the same radial distance (near 22R_J) albeit at the pre-midnight sector (LT ~21–22 h), the >1 MeV enhancement disappears. However, the previously weak enhancement of >11 MeV electrons becomes much greater, and just inward of this enhancement, what is even more noticeable is the emergence of a new peak of >11 MeV rates at ~19R_J as denoted by the two vertical dashed lines marked with L1 and L2. The peak count-rate of > 11 MeV transients is about 50 times above the average value. The γ parameter is 17.6, indicating that this event is dominated by >11 MeV electrons. Nevertheless, there is little response or even a slight decrease in the flux intensities of the four 100 s of keV channels, as shown in Figure 2d. Some of the missing F0–F3 measurements near L1 are due to contamination of the respective channels by the same electrons that form the >11 MeV transient.

3.2.2 Orbit C9: enhancements at both >1 and >11 MeV

Figure 3a presents two transient extensions observed during the inbound crossing of orbit C9: one at the >11 MeV channel and the other at the >1 MeV channel. Both events were detected at the dawn sector with LT ~5–6 h, from 9:38 in day 176 to 3:14 in day 177 of 1997. There are two peaks in the radial profile at ~27R_J and ~23R_J, respectively, for both events, with a sharp drop in intensity at L ~24–25R_J. Taking into account both peaks, the two events during orbit C9 span as wide as 7R_J in the radial direction, making them the broadest in spatial range across all transient events.

The peak count-rate is ~45 times above the average for the >11 MeV transient and is ~37 times above the average for the >1 MeV transient. The parameter γ of ~0.9 further confirms that the enhancements of both >11 and >1 MeV electrons are comparable in importance during the orbit C9 event. Figure 3b shows the corresponding radial distributions of channels F0, F1, F2, and F3. Prominent enhancements of these 100s of keV electron intensities can be found at ~22–27R_J, the same radial distance as the >11 and >1 MeV transients.

3.2.3 Orbit E4: enhancement at >1 MeV

Figure 4a shows the transient extension of >1 MeV electrons observed during the E4 orbit inbound crossing at the dawn sector with LT ~8 h, from 8:24 to 12:23 on day 352 of 1996. We see that while the >11 MeV rates follow the long-term average trend of decreasing toward larger radial distance, there is a clear enhancement in the >1 MeV count-rates. Such dominance of >1 MeV enhancement is confirmed by the parameter γ of ~0.4. The transient event spans ~1.6R_J in radial distance, with its maximum at ~23.5R_J. The peak count-rate is ~13 times above the average, rendering this event a relatively weak one among all transient extensions. Accompanied by the >1 MeV electron enhancement are significant increases in the flux intensities of 100 s of keV electrons at the same radial distance, as shown in Figure 4b.

3.3 Statistical Analyses

3.3.1 The distribution of the occurrence of transient extensions with radial distance, LT, and epoch

Figure 5 shows the distribution of the occurrence of transient extensions with radial distance and LT, based on information about the location of transient events shown in Table 1. Figure 5a reveals that the >11 MeV transients mainly occur at ~20 ± 5R_J. Another important feature is a clear LT asymmetry, with three transient events appearing in the dawn sector at LT ~6 h, and one event in the post-dusk sector at LT ~21 h. Figure 5b shows that the >1 MeV transients are also mostly located around ~20R_J, but they have never been found at a radial distance as small as ~15R_J, where Galileo detected one >11 MeV transient during orbit C22. Figure 5) reveals a clear dawn-dusk asymmetry of the occurrence of >1 MeV transients. There are four events detected in the dawn

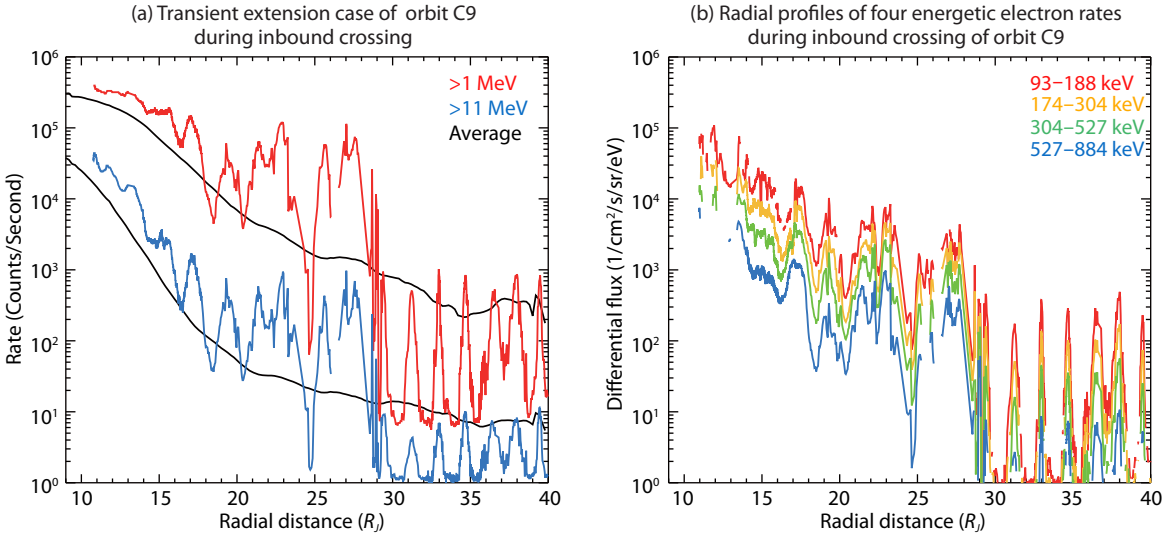

Figure 3. The transient extensions of both >11 MeV and >1 MeV electrons discovered during the inbound crossing of orbit C9. The radial profiles are from day 174 to 178 in 1997. The format is the same as Figure 2.

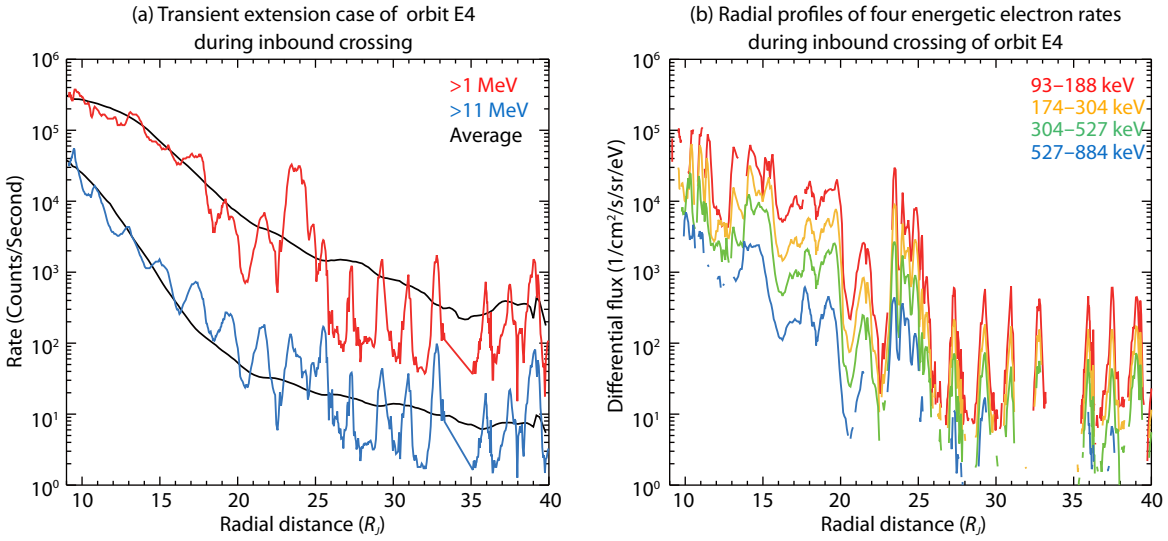

Figure 4. The transient extension of >1 MeV electrons discovered during the inbound crossing of orbit E4. The radial profiles are from day 350 to 354 in 1996. The format is the same as Figure 2.

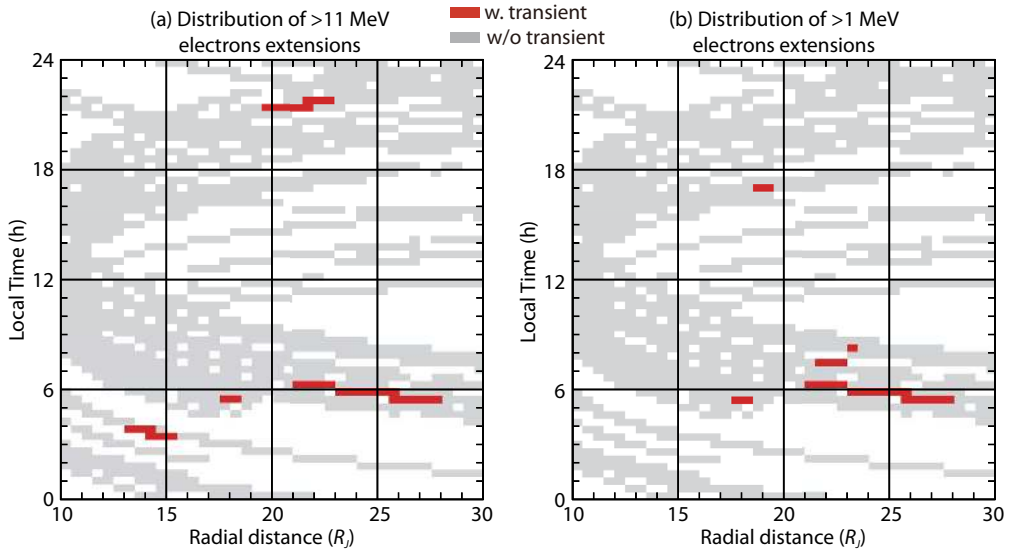

Figure 5. The distribution of the occurrence of transient extensions with radial distance and LT. We set each spatial grid as 0.5R_J in radial distance and 0.4 h in LT. Grids within which Galileo spacecraft detected transient extensions are filled in red, while grey indicates the regions covered by Galileo's trajectories with EPD on, but with no transient events discovered. White regions indicate that there is no measurement throughout the mission.

sector around LT ~6 h, yet only one event in the dusk sector at LT ~17 h. It is notable that all the transients occur before the year 2000. While all these hints of spatial asymmetries and temporal variations rely on only a few events, they are still noteworthy and will be further discussed in Section 4.

3.3.2 Correlation between the variations of MeV and 100 s of keV electrons

In each panel of Figure 6, we plot F0–F3 fluxes against simultaneous measurements by the LEMMS channels DC2 (>1 MeV) and DC3 (>11 MeV). In all panels, black dots show quiescent time periods (Galileo crossings with no transients), and colored crosses (dots) denote periods with transients, within (outside) the full width at 10% maximum of the transients. Figure 6a, c, e, and g reveal that the intensities sampled during the crossings with >1 MeV transient events (in red) approximately follow the linear trend of the Galileo crossings without the >1 MeV transients (black dots fitted by the green line). However, Figure 6b, d, f, and h show notable deviations during transient periods, compared to a linear trend that is indicative of quiet times. The intensities within the full width at 10% maximum of transients (blue crosses) exhibit a tendency toward much greater enhancements of >11 MeV intensities than for 100 s of keV intensities. Note that in Figure 6h, the data points corresponding to the >11 MeV transient are absent during orbit C22, because the 527–884 keV count-rates were contaminated by penetrating electrons.

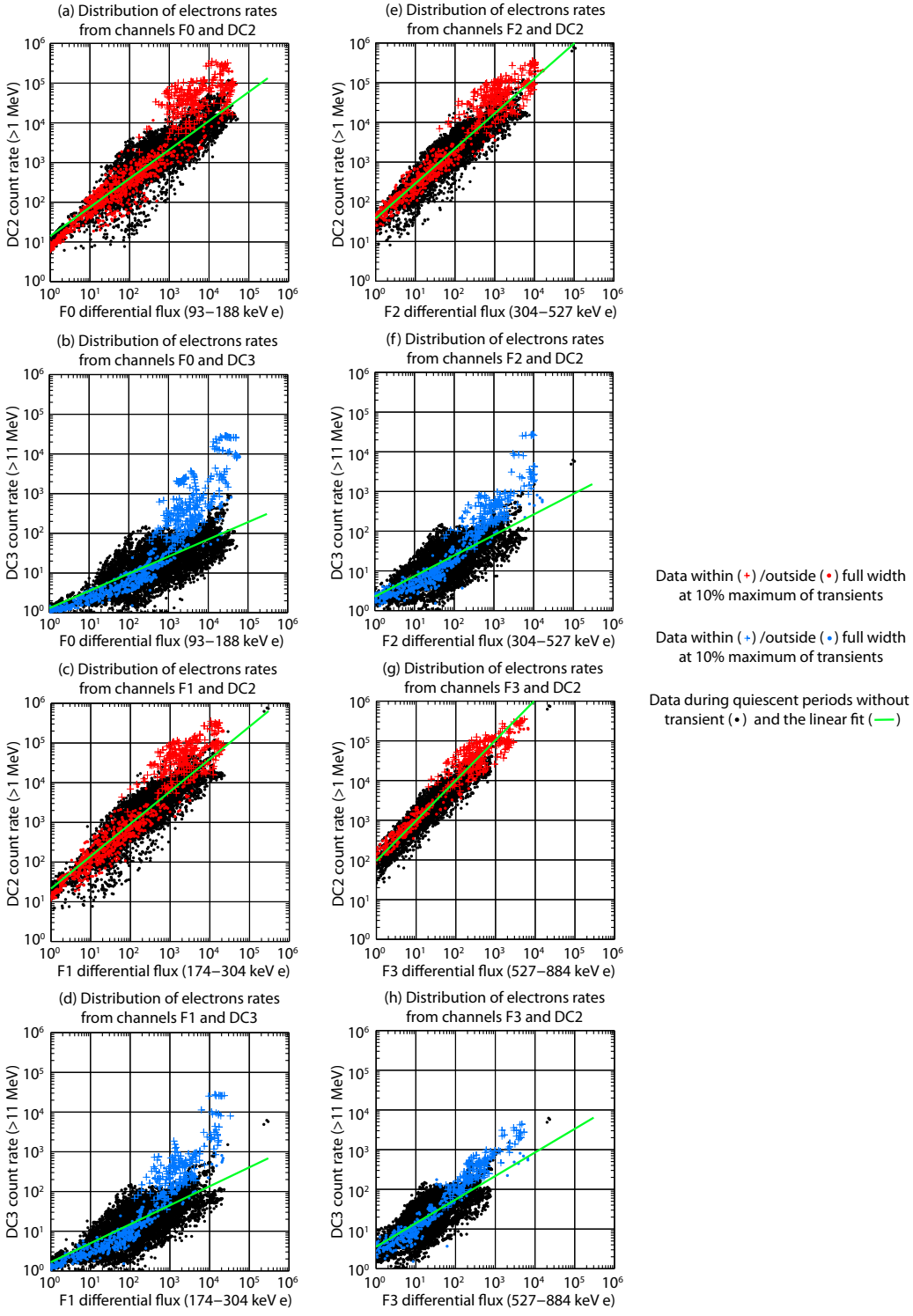

Figure 6. The scatter plots of >1 and >11 MeV electron count-rates versus the 100s of keV electron differential fluxes. Panel (a): The scatter plot of >1 MeV count-rates versus 93–188 keV differential fluxes. Red represents data from the Galileo crossings with >1 MeV transient extensions. For each case, we select the measurements from the radial distance at the inner boundary of the full width at 10% maximum of the transient event, to 40R_J. Red crosses denote the measurements within the full width at 10% maximum of the transients, and red solid dots represent the other measurements. Black dots are from the Galileo crossings without >1 MeV transients, for the radial distance range from 18R_J to 40R_J. The green straight line shows the linear fit of the black dots. Panels (c), (e), and (g) show the scatter plots of >1 MeV count-rates versus 174–304 keV, 304–527 keV, and 527–884 keV differential fluxes, respectively. The format is the same as panel (a). Panel (b): The scatter plot of >11 MeV count-rates versus 93–188 keV differential fluxes. The format is the same as panel (a), except that blue (black) represents the data from crossings with (without) the >11 MeV transients. Panels (d), (f), and (h) show the scatter plots of >11 MeV count-rates versus 174–304 keV, 304–527 keV, and 527–884 keV differential fluxes, respectively. The format is the same as panel (b).

4. Discussion

In this study, we investigated the radial distributions of intensities for >11 MeV and >1 MeV relativistic electrons observed by Galileo and compared them with those of 100 s of keV energetic electrons. The long-term average distribution of relativistic electrons presents a trend of monotonic decrease with increasing radial distance. However, our detailed orbit-by-orbit survey reveals that pronounced enhancements of relativistic electron intensities, namely transient extensions, could significantly distort the long-term trend. Transient extensions have been discovered during seven Galileo crossings, demonstrating that the C22 event was not a single extreme transient and should not be studied in isolation.

We note that the relatively small number of transient extensions does not necessarily mean that their occurrence is rare; rather, there are only a total of 34 orbits (68 inbound or outbound crossings) with EPD on during the entire mission. The total spacecraft dwell time between $10R_J$ and $30R_J$ is about 57 days. Given that we found transients during seven Galileo crossings, a rough estimate of the occurrence frequency is about one transient every eight days. This limitation due to incomplete orbital coverage is even more important if we consider that the detection probability depends on the local time of Galileo, because certain orbits did not sample either dawn or dusk to where the seven events map. An estimate of occurrence frequency at dawn is once per three days, considering the dwell time of Galileo at $3 \le \mathrm{LT} \le 8$ and between $10R_J$ and $30R_J$. This time scale is similar to that of periodic energetic particle bursts and plasma sheet thinning (Krupp et al., 1998; Woch et al., 1998, 2002).

Our statistical analyses show that transient extensions mainly occur at a radial distance of $\sim 20 \pm 5R_J$. There is a noticeable dawn-dusk asymmetry of the occurrence of transient extensions, with the majority of events appearing in the dawn sector, which may also be subject to time variability. In the following subsections, we will discuss possible mechanisms for transient extensions and their dawn-dusk asymmetry.

4.1 The Combined Effect of Injections and Convective Transport

The case of >11 MeV transient extension during orbit C22 was postulated to be the result of enhanced radial diffusion due to the intense but rare volcanic activity of Io (Russell et al., 2001). However, our finding of a number of other transient events indicates that this is not likely the cause. Recently, Hao et al. (2020) studied the C22 event by simulating the motion of electrons as a result of magnetic drifts, corotation, and an $\boldsymbol{E} \times \boldsymbol{B}$ drift attributed to a uniform yet temporally variable large-scale dawn-dusk electric field. The simulation suggested that electrons with energies close to the corotation-drift-resonant energy ($\boldsymbol{E}_{\mathrm{CDR}}$) can be effectively transported and accelerated by the changes of large-scale electric field. This is because the magnetic drifts of electrons around $\boldsymbol{E}_{\mathrm{CDR}}$ to a large extent cancel out the corotation, so they drift very slowly in LT (Birmingham, 1982; Guio et al., 2020). As a result, these electrons can be easily transported by the enhancements of a large-scale electric field which impose radial flows at fixed LT sectors, and accelerate the electrons adiabatically. Hao et al. (2020) also modeled the radial distributions of >11 MeV and >1 MeV intensities (from DC3 and DC2 channels, respectively) during orbit C22. The simulation successfully reconstructed the observed key features of the >11 MeV transient extension, most importantly the stronger enhancement of the >11 MeV electron channel of EPD compared to the >1 MeV one. The former receives larger fractional contribution from near-$\boldsymbol{E}_{\mathrm{CDR}}$ electrons, since $\boldsymbol{E}_{\mathrm{CDR}}$ at the location of the C22 transient is near 10 MeV. Therefore, the simulation appears consistent with the inference that >11 MeV transient extension during orbit C22 essentially results from convective transport due to a large-scale electric field. It should be noted that for the development of the transients, the variability, the magnitude of the electric field are the most determinant, rather than its orientation, as suggested by similar simulations for Saturn (Roussos et al., 2018; Hao et al., 2020).

What Hao et al. (2020) did not discuss is whether this electric field can also drive strong LT asymmetries in the distribution of transients by modifying the otherwise circular, circumplanetary bounce-averaged drift trajectory of their electrons. To illustrate how the electric field may affect the drift trajectories, we have simulated the contours of constant first adiabatic invariant (μ) for the drifts of equatorially mirroring electrons, as shown in Figure 7. The electric field is set as constant and uniform in the dawn-dusk direction, and the magnetic field is set as a dipole field. Since we aim to qualitatively assess the drifts of electrons at radial distance $\le \sim 20R_J$, the dipole approximation generally fulfills our needs. As electrons undergo adiabatic drifts, their trajectories follow the constant-μ contours. Thus, Figure 7 is representative of the drift

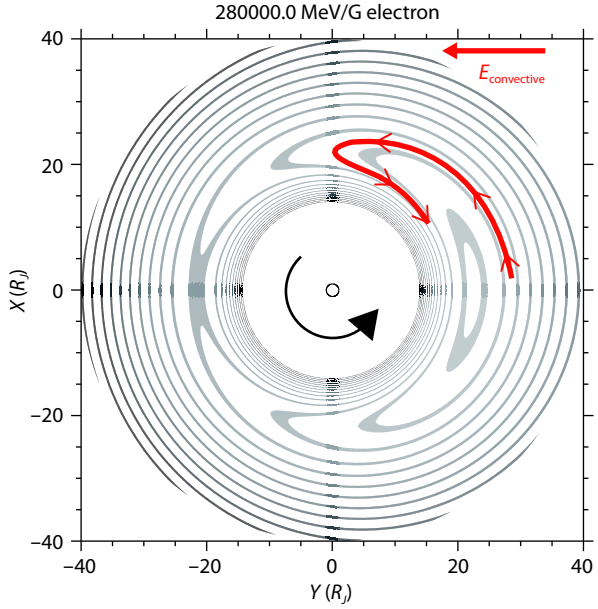

Figure 7. The simulation result of the bounce-averaged drift trajectory in the *X*-*Y* plane of JSE coordinate, of electrons with the first adiabatic invariant (μ) of 280000 MeV/G marked by the red curve with arrows. The simulation assumes a dipole magnetic field. The grey curves indicate the contours of constant μ. The red arrow at the upper right corner denotes the direction of the Jovian convective electric field. The black arrow at the center shows the direction of magnetospheric corotation.

trajectories of electrons. We set the first adiabatic invariant of the electrons as 280000 MeV/G, corresponding to $\boldsymbol{E}_{\rm CDR}$ at ~20R_J, and launch the electrons at ~20R_J. We take the radial distance of ~20R_J based on our observations. An additional reason is that at this distance range (20–30R_J), there exist acceleration sites of MeV ions (Selesnick et al., 2001) and possibly lower-energy ions and energetic electrons (Krupp et al., 1998; Woch et al., 1998, 2002). The drift trajectory varies depending on the LT at which the electrons are launched. The red curve in Figure 7 marks the trajectory of electrons launched at LT ~6 h. These electrons would be trapped along a closed trajectory and are not able to execute circumplanetary drift. While there is both inward and outward electron transport along such closed trajectories, the net effect is that of an inward transport and acceleration, since Garrett and Jun (2021) showed falling PSD profiles towards Jupiter on average.

Thus, even if the acceleration that triggers the injection of electrons develops uniformly in LT, the dawn-dusk electric field would force the dawn-side injected electrons with energies around $\boldsymbol{E}_{\rm CDR}$ to reside for longer around dawn and contribute to the observed LT asymmetry. A similar explanation has been offered for the LT-restricted location of a micro-radiation belt component observed near Saturn's main rings (Roussos et al., 2019). This explanation would be applicable for a range of radial distances and energies, since $\boldsymbol{E}_{\rm CDR}$ is L-shell dependent.

A caveat of the aforementioned explanation is that the dawn-dusk electric field has only been indirectly observed near the orbit of Io at ~6R_J (Barbosa & Kivelson, 1983; Ip & Goertz, 1983; Murakami et al., 2016). Therefore, it remains unclear to what extent the dawn-dusk electric field alone could lead to the dawn-dusk asymmetry of the transient extensions. Furthermore, the occurrences of transients with comparable enhancements at both >1 MeV and >11 MeV channels suggest that their generation and distribution are also controlled by other processes with a propensity at dawn.

There are a number of studies suggesting a preferential acceleration of energetic particles in the dawnside magnetosphere compared to the duskside. Krupp et al. (1998), Woch et al. (1998), and Woch et al. (2002) investigated bursts of energetic electrons and ions with a period of 2–3 days in the mid- to outer magnetosphere. In particular, Woch et al. (2002) found that bursts in the radial direction mainly occur at the dawn sector, and the inward bursts tend to appear at a smaller radial distance, whereas the outward ones tend to be further away from the planet. This suggests that the bursts could be related to near-Jupiter reconnection (Vasyliunas, 1983; Kronberg et al., 2005). Vogt et al. (2010) and Vogt et al. (2020) identified reconnection events in the middle and outer magnetosphere observed by Galileo and Juno, revealing that a similar LT asymmetry of predominant occurrence at dawn also exists for the reconnection sites. Recently, Yao et al. (2020) and Swithenbank-Harris et al. (2021) analyzed the storm-time dynamics at dawn in the context of auroral emissions, suggesting that inward bursts of energetic electrons and protons associated with reconnection could be linked to common occurrences of auroral dawn storms in Jovian magnetosphere (Grodent et al., 2018). Similar local time asymmetries of storm-time dynamics and associated injections have also been observed in Saturn's magnetosphere. Mitchell et al. (2009) investigated the recurrent ring current enhancements revealed by Cassini ENA measurements and found that they occur preferentially at dawn. Mitchell et al. (2009) further showed that ring current enhancements are closely related to Saturn Kilometric Radiation (SKR) enhancements and dawnward auroral UV emissions. Mitchell et al. (2009) accordingly proposed that reconnection in the plasma sheet of Saturn's magnetosphere may be responsible for these recurrent events at dawn.

All of the above research indicates that there is a broad charged particle acceleration region in Jupiter's middle magnetosphere (or fast rotating, mass loaded magnetospheres in general) with a preferential dawnward extension. The topology of the relativistic electron transients and the characteristic few day time scale associated with their appearance could hint that their origin is connected to this region, as well as to the storm-time dynamics at dawn and the energetic particle bursts associated with dipolarizations reported by other Galileo observations. Contributions to the dawn-dusk asymmetry may further originate from convective flows associated with the dawn-dusk electric field at Jupiter, if that extends to greater distances than Io's torus. This, or any other convective electric field, may nevertheless be responsible for transporting the transient electron enhancements from their generation at 20–25R_J towards the inner magnetosphere, giving rise to extreme events like C22.

Furthermore, energy diffusion due to interaction with whistler waves may also lead to electron acceleration at MeV energies (Woodfield et al., 2014), but such wave-particle interactions may only play a major role at a smaller radial distance (L < 20), where the wave intensities become significant (Menietti et al., 2016). Furthermore, Kollmann et al. (2018) found that at L > 20 the MeV electrons are dominated by adiabatic heating coupled with radial transport, whereas acceleration due to wave-particle interaction may be a minor effect. Thus, in the middle magnetosphere where most of the transient events occurred, we suggest that adiabatic acceleration associated with convective radial transport and injections is primarily responsible for the transients at MeV energies. The non-adiabatic acceleration due to the interaction of electrons with plasma waves may contribute to the observed MeV electrons, but may not the dominant process.

4.2 Temporal Variations of Upstream Solar Wind and Interplanetary Magnetic Field

In this subsection, we discuss the possibility that the dawn-dusk asymmetry could be a misleading characteristic due to long-term temporal variations of the upstream solar wind and interplanetary magnetic field (IMF) conditions. Table 1 shows that all transient events were detected before the year 2000, which falls mostly within the ascending phase of Solar Cycle 23 towards solar maximum. Thus, if the solar wind and IMF conditions varied significantly after 2000, there would be a question as to whether such changes could affect the occurrence of transient extensions.

To assess the potential influence of solar wind variations, we need to acquire upstream solar wind and IMF conditions. Since there are no continuous solar wind and IMF measurements throughout the entire Galileo mission, we utilized two MHD models which

propagate solar wind conditions from Earth's orbit at 1 AU to Jupiter's orbit at 5.2 AU: the Michigan Solar Wind Model (mSWiM) (Zieger and Hansen, 2008) and the Tao model (Tao et al., 2005). The latter restricts the simulation to only periods of alignment or opposition between Earth and Jupiter (the difference in helioecliptic longitude ≤ ±90°), whereas the former provides solutions for the non-optimal alignment of Jupiter and Earth.

We present histograms of solar wind and IMF parameters before and after the year of 2000 in Figure 8. The total magnetic field strength and the tangential component of IMF arederived from the mSWiM model, while the solar wind dynamic pressure (P_{dyn}), proton density, and velocity are used from both the mSWiM and Tao models. Other parameters such as solar wind temperature and the normal component of IMF with reference to the ecliptic plane are not plotted, as their prediction efficiencies are relatively low (Zieger and Hansen, 2008). Figure 8 reveals that there is no obvious difference between P_{dyn} before and after 2000, whereas

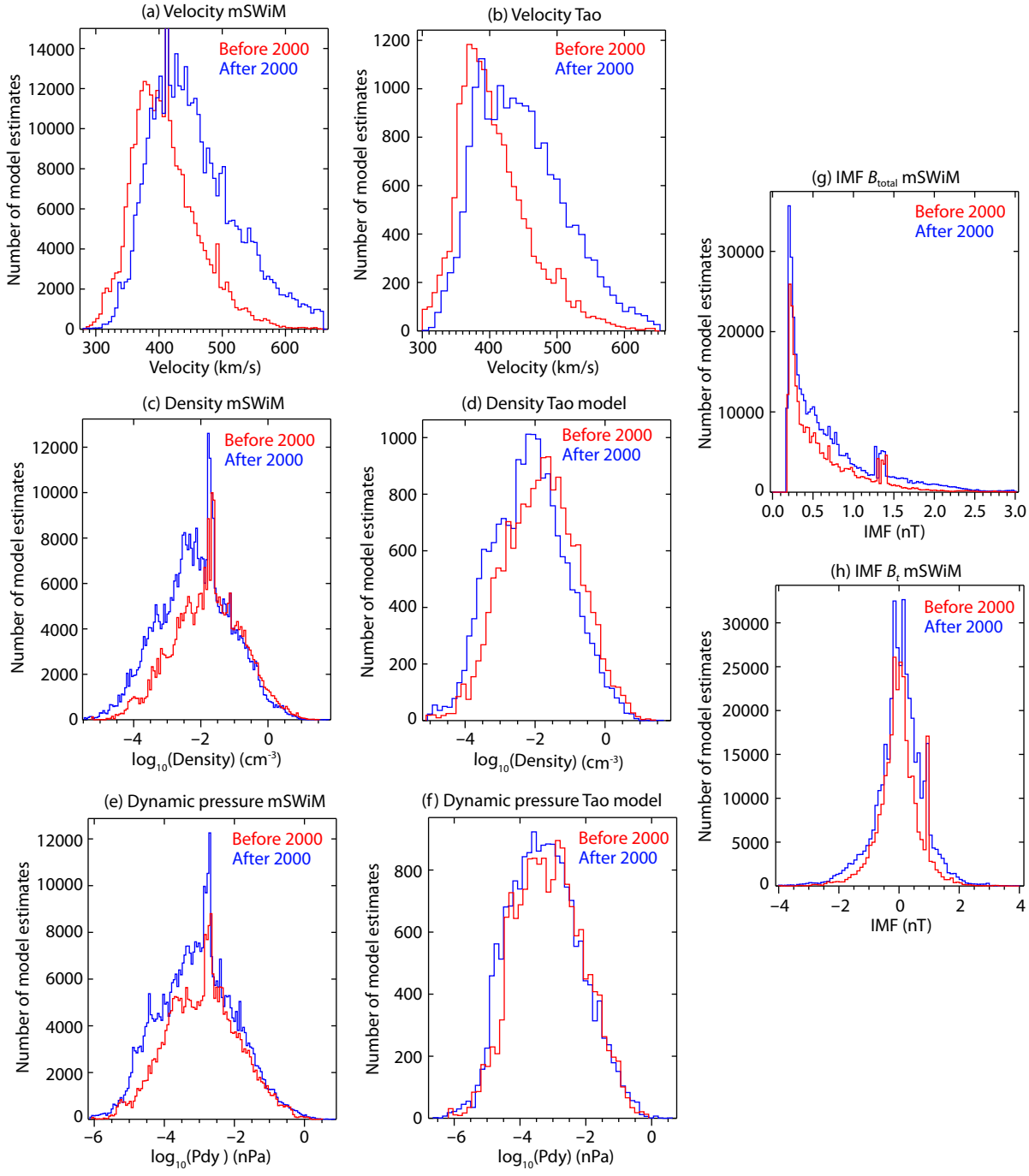

Figure 8. Histograms of the modeled upstream IMF and solar wind conditions of the Jovian magnetosphere. Red represents results before the year 2000, and blue represents those after 2000. (a), (c), (e), (g), and (h): The mSWiM model results for solar wind velocity, proton density, dynamic pressure, total magnetic field, and the tangential component of IMF in Radial-Tangential-Normal coordinates, respectively. (b), (d), and (f): the Tao model results for solar wind velocity, proton density, dynamic pressure, respectively.

after 2000, the solar wind velocities systematically shift to higher values and proton densities shift to lower values. One possibility is that the corotation interaction regions (CIRs) and high speed streams of solar wind may gradually become significant when Solar Cycle 23 evolves into its descending phase. However, since the transition to the descending phase occurred around and after the end of the Galileo mission, variations in solar wind velocity and density would likely not influence the observation of transient events.

We also examined the variations of P_{dyn} during all 34 Galileo orbits throughout the mission, as P_{dyn} has been shown to be particularly effective in triggering the responses in the mid- to outer Jovian magnetosphere (Ebert et al., 2014; Vogt et al., 2019, and references therein). The P_{dyn} enhancement events are from the event list in Vogt et al. (2019). We define the range in LT and radial distance (R) for the dawn region as $3\,\mathrm{h} \le$ LT $\le 8\,\mathrm{h}$ and $15R_J \le R \le 30R_J$, and for the dusk region as $16\,\mathrm{h} \le$ LT $\le 22\,\mathrm{h}$ and $15R_J \le R \le 30R_J$. For each dawn or dusk crossing, we set t_1 as 5 days prior to entering the dawn/dusk region, and t_2 as 1 day after exiting the region. We assume the time scale of t_1 is five days, because the transient extension may have already existed for hours or a few days before being detected by Galileo, so there could be a time lag between the P_{dyn} perturbation and the responses in the middle and inner magnetosphere. We assume the time scale of t_2 is one day, because the uncertainty of the model's prediction could be one day at the exact time of the arrival of P_{dyn} perturbation at Jupiter's magnetosphere. If there is a P_{dyn} enhancement occurring during the time period from t_1 to t_2, then we associate the P_{dyn} enhancement with the crossing. Next, we collectively review our results to explore whether such associations may be meaningful or coincidental. The time sequence plots of the modeled solar wind proton density, velocity, and P_{dyn} during each of the 34 Galileo orbits are provided as supplementary materials. In the supplementary plots, the P_{dyn} enhancements are shaded blue, and the time period corresponding to the dawn (dusk) region is marked with vertical dashed light blue (black) lines. The occurrence of transient events is indicated by vertical solid blue lines.

Orbits G2 to C22 (September 1996 to August 1999) crossed both the dawn and dusk regions during one perijove approach. For each of these orbits, we group two successive crossings as one pair. We then find that there are 12 such crossing pairs associated with P_{dyn} enhancements. Among these 12 crossing pairs, we found transient extensions during the dawn crossings of orbits E4, C9, and C22, but no transient events during the dusk counterparts. For those orbits not associated with P_{dyn} enhancement, there is a transient extension during orbit E17, but it was detected only during the dawn crossing. These results are supportive of the view that the dawn-dusk asymmetry is not caused by variations of P_{dyn}.

During orbit G1 (June 1996) and orbits C23 to A34 (from September 1999 to November 2002), Galileo did not travel through the dawn region between $15R_J$ and $30R_J$, and only the dusk region was visited. For orbit G1, the dusk crossing is associated with P_{dyn} enhancements, but not with transient extensions. Orbits C23 to A34 coincided with the transition of Solar Cycle 23 from maximum to the descending phase. For these orbits, we find nine dusk crossings associated with P_{dyn} enhancements (only the one during orbit I24 had a transient extension). The total number of nine is less than that of thirteen for orbits G1 to C22, although this difference may not be the result of changes in P_{dyn}. Instead, it may be due to the fact that the final few orbits had longer periods, and thus spent less time in the regions of interest. Figure 8e and f also suggest that there is no pronounced difference in P_{dyn} conditions before and after 2000. These results suggest that after 2000, although the dawn region could not be sampled by Galileo, the lack of transient extensions at dusk is not the temporal effect of changes in P_{dyn}.

Therefore, although we cannot exclude the possibility that solar wind conditions may affect the dynamics of Jupiter's electron radiation belts (Han et al., 2018; Hao et al., 2020), it seems that the temporal effects of solar wind and IMF conditions are not likely to be the root cause behind the lack of transients after 2000; rather, the combined effects of local time asymmetry and orbital coverage effects by Galileo serve as the most probable explanation for the observed distribution of transients in space and time.

5. Conclusion

Through an orbit-by-orbit inspection of observations by Galileo from 1996 to 2002, we found transient enhancements of MeV electron intensities during seven crossings, all before the year 2000. Transient events mainly occurred at ~$20 \pm 5R_J$. A remarkable feature of their spatial distribution is the dawn-dusk asymmetry, with most of the events occurring at dawn. The dawn-dusk asymmetry of MeV electron transients and their recurrence time scale of a few days imply their potential relationship to energetic particle bursts in the mid- and outer magnetosphere. We posit that transient enhancements, as well as the dawn-dusk asymmetry, may result from a synergy between convective transport due to the large-scale dawn-dusk electric field and injections at a broad region in the middle, dawnside magnetosphere. The temporal effect of variations in solar wind conditions is also discussed, and is considered unlikely to be responsible for the distribution of transient events in the Jovian electron radiation belt.

Acknowledgments

We acknowledge support from the China Space Agency's project D020303. This work is also supported by the Strategic Priority Research Program of the Chinese Academy of Sciences (Grant No. XDA17010201), the Key Research Program of the Institute of Geology & Geophysics, Chinese Academy of Sciences, Grant No. IGGCAS-201904, and by the National Natural Science Foundation of China (42074200, 42030202 and 41774161). We thank P. Kollmann (JHUAPL), C. Paranicas (JHUAPL), A. Lagg (MPS), Z. H. Lee-Payne (Aberytwyth University), M. Kusterer (JHUAPL), D. Smith (JHUAPL) and J. Vandegriff (JHUAPL) for processing and delivering Galileo EPD data. EPD/LEMMS data utilized in this study can be obtained at http://sd-www.jhuapl.edu/Galileo_EPD/latest_calibrated_data/.

References

Andriopoulou, M., Roussos, E., Krupp, N., Paranicas, C., Thomsen, M., Krimigis, S., Dougherty, M. K., and Glassmeier, K. H. (2012). A noon-to-midnight electric field and nightside dynamics in Saturn's inner magnetosphere, using

microsignature observations. *Icarus*, *220*(2), 503–513. https://doi.org/10.1016/j.icarus.2012.05.010

Andriopoulou, M., Roussos, E., Krupp, N., Paranicas, C., Thomsen, M., Krimigis, S., Dougherty, M. K., and Glassmeier, K. H. (2014). Spatial and temporal dependence of the convective electric field in Saturn's inner magnetosphere. *Icarus*, *229*, 57–70. https://doi.org/10.1016/j.icarus.2013.10.028

Barbosa, D. D., and Kivelson, M. G. (1983). Dawn-dusk electric field asymmetry of the Io plasma torus. *Geophys. Res. Lett.*, *10*(3), 210–213. https://doi.org/10.1029/GL010i003p00210

Birmingham, T. J. (1982). Charged particle motions in the distended magnetospheres of Jupiter and Saturn. *J. Geophys. Res.*, *87*(A9), 7421–7430. https://doi.org/10.1029/JA087iA09p07421

Bolton, S. J., Janssen, M., Thorne, R., Levin, S., Klein, M., Gulkis, S., Bastian, T., Sault, R., Elachi, C., … West, R. (2002). Ultra-relativistic electrons in Jupiter's radiation belts. *Nature*, *415*(6875), 987–991. https://doi.org/10.1038/415987a

Drake, F. D., and Hvatum, S. (1959). Non-thermal microwave radiation from Jupiter. *Astron. J.*, *64*, 329–330. https://doi.org/10.1086/108047

Ebert, R. W., Bagenal, F., McComas, D. J., and Fowler, C. M. (2014). A survey of solar wind conditions at 5 AU: a tool for interpreting solar wind-magnetosphere interactions at Jupiter. *Front. Astron. Space Sci.*, *1*, 4. https://doi.org/10.3389/fspas.2014.00004

Fillius, R. W., and McIlwain, C. E. (1974). Measurements of the Jovian radiation belts. *J. Geophys. Res.*, *79*(25), 3589–3599. https://doi.org/10.1029/JA079i025p03589

Garrett, H. B., and Jun, I. (2021). First adiabatic invariants and phase space densities for the Jovian electron and proton radiation belts—Galileo and GIRE3 estimates. *J. Geophys. Res.*, *126*(1), e2020JA028593. https://doi.org/10.1029/2020JA028593

Grodent, D., Bonfond, B., Yao, Z., Gérard, J. C., Radioti, A., Dumont, M., Palmaerts, B., Adriani, A., Badman, S. V., … Valek, P. (2018). Jupiter's aurora observed With HST During Juno orbits 3 to 7. *J. Geophys. Res.*, *123*(5), 3299–3319. https://doi.org/10.1002/2017JA025046

Guio, P., Staniland, N. R., Achilleos, N., and Arridge, C. S. (2020). Trapped particle motion in Magnetodisk fields. *J. Geophys. Res.*, *125*(7), e2020JA027827. https://doi.org/10.1029/2020JA027827

Han, S., Murakami, G., Kita, H., Tsuchiya, F., Tao, C., Misawa, H., Yamazaki, A., and Nakamura, M. (2018). Investigating solar wind-driven electric field influence on long-term dynamics of Jovian synchrotron radiation. *J. Geophys. Res.*, *123*(11), 9508–9516. https://doi.org/10.1029/2018JA025849

Hao, Y. X., Sun, Y. X., Roussos, E., Liu, Y., Kollmann, P., Yuan, C. J., Krupp, N., Paranicas, C., Zhou, X. Z., and Murakami, G. (2020). The Formation of Saturn' s and Jupiter's electron radiation belts by Magnetospheric electric fields. *Astrophys. J. Lett.*, *905*(1), L10. https://doi.org/10.3847/2041-8213/abca3f

Ip, W. H., and Goertz, C. K. (1983). An interpretation of the dawn–dusk asymmetry of UV emission from the Io plasma torus. *Nature*, *302*(5905), 232–233. https://doi.org/10.1038/302232a0

Jun, I., Garrett, H. B., Swimm, R., Evans, R. W., and Clough, G. (2005). Statistics of the variations of the high-energy electron population between 7 and 28 Jovian radii as measured by the Galileo spacecraft. *Icarus*, *178*(2), 386–394. https://doi.org/10.1016/j.icarus.2005.01.022

Khurana, K. K. (1992). A generalized hinged-magnetodisc model of Jupiter's Nightside current sheet. *J. Geophys. Res.*, *97*(A5), 6269–6276. https://doi.org/10.1029/92JA00169

Kollmann, P., Roussos, E., Paranicas, C., Woodfield, E. E., Mauk, B. H., Clark, G., Smith, D. C., and Vandegriff, J. (2018). Electron acceleration to MeV energies at Jupiter and Saturn. *J. Geophys. Res.*, *123*(11), 9110–9129. https://doi.org/10.1029/2018JA025665

Kollmann, P., Paranicas, C., Lagg, A., Roussos, E., Lee-Payne, Z. H., Kusterer, M., Smith, D., Krupp, N., and Vandegriff, J. (2020). Galileo/EPD user guide. Retrieved from https://doi.org/10.1002/essoar.10503620.1.

Kronberg, E. A., Woch, J., Krupp, N., Lagg, A., Khurana, K. K., and Glassmeier, K. H. (2005). Mass release at Jupiter: Substorm-like processes in the Jovian magnetotail. *J. Geophys. Res.*, *110*(A3), A03211. https://doi.org/10.1029/2004JA010777

Krupp, N., Woch, J., Lagg, A., Wilken, B., Livi, S., and Williams, D. J. (1998). Energetic particle bursts in the predawn Jovian magnetotail. *Geophys. Res. Lett.*, *25*(8), 1249–1252. https://doi.org/10.1029/98GL00863

Menietti, J. D., Groene, J. B., Averkamp, T. F., Horne, R. B., Woodfield, E. E., Shprits, Y. Y., de Soria-Santacruz Pich, M., and Gurnett, D. A. (2016). Survey of whistler mode chorus intensity at Jupiter. *J. Geophys. Res.*, *121*(10), 9758–9770. https://doi.org/10.1002/2016JA022969

Mitchell, D. G., Krimigis, S. M., Paranicas, C., Brandt, P. C., Carbary, J. F., Roelof, E. C., Kurth, W. S., Gurnett, D. A., Clarke, J. T., … Pryor, W. R. (2009). Recurrent energization of plasma in the midnight-to-dawn quadrant of Saturn's magnetosphere, and its relationship to auroral UV and radio emissions. *Planet. Space Sci.*, *57*(14-15), 1732–1742. https://doi.org/10.1016/j.pss.2009.04.002

Murakami, G., Yoshioka, K., Yamazaki, A., Tsuchiya, F., Kimura, T., Tao, C., Kita, H., Kagitani, M., Sakanoi, T., … Fujimoto, M. (2016). Response of Jupiter's inner magnetosphere to the solar wind derived from extreme ultraviolet monitoring of the Io plasma torus. *Geophysical Research Letters*, *43*(24), 12308–12316. https://doi.org/10.1002/2016GL071675

Northrop, T. G., Goertz, C. K., and Thomsen, M. F. (1974). The magnetosphere of Jupiter as observed with Pioneer 10: 2. Nonrigid rotation of the magnetodisc. *J. Geophys. Res.*, *79*(25), 3579–3582. https://doi.org/10.1029/JA079i025p03579

Paranicas, C., Mitchell, D. G., Roussos, E., Kollmann, P., Krupp, N., Müller, A. L., Krimigis, S. M., Turner, F. S., Brandt, P. C., … Johnson, R. E. (2010). Transport of energetic electrons into Saturn's inner magnetosphere. *J. Geophys. Res.*, *115*(A9), A09214. https://doi.org/10.1029/2010JA015853

Roussos, E., Kollmann, P., Krupp, N., Paranicas, C., Dialynas, K., Sergis, N., Mitchell, D. G., Hamilton, D. C., and Krimigis, S. M. (2018). Drift-resonant, relativistic electron acceleration at the outer planets: Insights from the response of Saturn's radiation belts to Magnetospheric storms. *Icarus*, *305*, 160–173. https://doi.org/10.1016/j.icarus.2018.01.016

Roussos, E., Kollmann, P., Krupp, N., Paranicas, C., Dialynas, K., Jones, G. H., Mitchell, D. G., Krimigis, S. M., and Cooper, J. F. (2019). Sources, sinks, and transport of energetic electrons Near Saturn's Main Rings. *Geophys. Res. Lett.*, *46*(7), 3590–3598. https://doi.org/10.1029/2018GL078097

Russell, C. T., Fieseler, P. D., Bindshadler, D., Yu, Z. J., Joy, S. P., Khurana, K. K., and Kivelson, M. G. (2001). Large scale changes in the highly energetic charged particles in the region of the Io torus. *Advances in Space Research*, *28*(10), 1495–1500. https://doi.org/10.1016/S0273-1177(01)00552-X

Selesnick, R. S., Cohen, C. M. S., and Khurana, K. K. (2001). Energetic ion dynamics in Jupiter's plasma sheet. *J. Geophys. Res.*, *106*(A9), 18895–18905. https://doi.org/10.1029/2000JA000242

Simpson, J. A., Hamilton, D. C., McKibben, R. B., Mogro-Campero, A., Pyle, K. R., and Tuzzolino, A. J. (1974). The protons and electrons trapped in the Jovian dipole magnetic field region and their interaction with Io. *J. Geophys. Res.*, *79*(25), 3522–3544. https://doi.org/10.1029/JA079i025p03522

Sorensen, T. C., Armstrong, T. P., Pavanasam, A. G., and Taherion, S. (2005). Galileo energetic particle detector observations of the spatial distributions and energy spectra of >1 and >11 MeV electrons in the 10-40 RJ region of the Jovian magnetosphere. *Icarus*, *178*(2), 395–405. https://doi.org/10.1016/j.icarus.2005.07.006

Sun, Y. X., Roussos, E., Krupp, N., Zong, Q. G., Kollmann, P., and Zhou, X. Z. (2019). Spectral signatures of adiabatic electron acceleration at Saturn Through Corotation drift cancelation. *Geophys. Res. Lett.*, *46*(17-18), 10240–10249. https://doi.org/10.1029/2019GL084113

Swithenbank‐Harris, B. G., Nichols, J. D., Allegrini, F., Bagenal, F., Bonfond, B., Bunce, E. J., Clark, G., Kurth, W. S., Kurth, B. H., and Wilson, R. J. (2021). Simultaneous observation of an Auroral dawn storm with the Hubble space telescope and Juno. *J. Geophys. Res.*, *126*(4), e2020JA028717. https://doi.org/10.1029/2020JA028717

Tao, C., Kataoka, R., Fukunishi, H., Takahashi, Y., and Yokoyama, T. (2005). Magnetic field variations in the Jovian magnetotail induced by solar wind dynamic pressure enhancements. *J. Geophys. Res.*, *110*(A11), A11208. https://doi.org/10.1029/2004JA010959

Thomsen, M. F., Roussos, E., Andriopoulou, M., Kollmann, P., Arridge, C. S., Paranicas, C. P., Gurnett, D. A., Powell, R. L., Tokar, R. L., and Young, D. T.

(2012). Saturn's inner magnetospheric convection pattern: Further evidence. *J. Geophys. Res.*, *117*(A9), A09208. https://doi.org/10.1029/2011JA017482

Vasyliunas, V. M. (1983). Plasma distribution and flow. In A. J. Dessler (Ed.), *Physics of the Jovian Magnetosphere* (pp. 395-453). Cambridge: Cambridge University Press. https://doi.org/10.1017/CBO9780511564574.013

Vogt, M. F., Kivelson, M. G., Khurana, K. K., Joy, S. P., and Walker, R. J. (2010). Reconnection and flows in the Jovian magnetotail as inferred from magnetometer observations. *J. Geophys. Res.*, *115*(A6), A06219. https://doi.org/10.1029/2009JA015098

Vogt, M. F., Gyalay, S., Kronberg, E. A., Bunce, E. J., Kurth, W. S., Zieger, B., and Tao, C. (2019). Solar wind interaction with Jupiter's magnetosphere: A statistical study of Galileo in situ data and modeled upstream solar wind conditions. *J. Geophys. Res.*, *124*(12), 10170–10199. https://doi.org/10.1029/2019JA026950

Vogt, M. F., Connerney, J. E. P., DiBraccio, G. A., Wilson, R. J., Thomsen, M. F., Ebert, R. W., Clark, G. B., Paranicas, C., Kurth, W. S., … Bolton, S. J. (2020). Magnetotail reconnection at Jupiter: A survey of Juno magnetic field observations. *J. Geophys. Res.*, *125*(3), e2019JA027486. https://doi.org/10.1029/2019JA027486

Williams, D. J., McEntire, R. W., Jaskulek, S., and Wilken, B. (1992). The Galileo energetic particles detector. *Space Sci. Rev.*, *60*(1), 385–412. https://doi.org/10.1007/BF00216863

Woch, J., Krupp, N., Lagg, A., Wilken, B., Livi, S., and Williams, D. J. (1998). Quasi‐periodic modulations of the Jovian magnetotail. *Geophys. Res. Lett.*, *25*(8), 1253–1256. https://doi.org/10.1029/98GL00861

Woch, J., Krupp, N., and Lagg, A. (2002). Particle bursts in the Jovian magnetosphere: Evidence for a near-Jupiter neutral line. *Geophys. Res. Lett.*, *29*(7), 42-1–42-4. https://doi.org/10.1029/2001GL014080

Woodfield, E. E., Horne, R. B., Glauert, S. A., Menietti, J. D., and Shprits, Y. Y. (2014). The origin of Jupiter's outer radiation belt. *J. Geophys. Res.*, *119*(5), 3490–3502. https://doi.org/10.1002/2014JA019891

Yao, Z. H., Bonfond, B., Clark, G., Grodent, D., Dunn, W. R., Vogt, M. F., Guo, R. L., Mauk, B. H., Connerney, J. E. P., … Bolton, S. J. (2020). Reconnection- and Dipolarization-driven Auroral dawn storms and injections. *J. Geophys. Res.*, *125*(8), e2019JA027663. https://doi.org/10.1029/2019JA027663

Yuan, C. I., Roussos, E., Wei, Y., and Krupp, N. (2020). Sustaining Saturn's electron radiation belts through episodic, global-scale relativistic electron flux enhancements. *J. Geophys. Res.*, *125*(5), e2019JA027621. https://doi.org/10.1029/2019JA027621

Zieger, B., and Hansen, K. C. (2008). Statistical validation of a solar wind propagation model from 1 to 10 AU. *J. Geophys. Res.*, *113*(A8), A08107. https://doi.org/10.1029/2008JA013046